J. Canfield[1]
Mem. ASME
Computational Physics Division,
Los Alamos National Laboratory,
P.O. Box 1663, MS F605,
Los Alamos, NM 87544
e-mail: jessec@lanl.gov

N. Denissen
Computational Physics Division,
Los Alamos National Laboratory,
P.O. Box 1663, MS B218,
Los Alamos, NM 87544
e-mail: denissen@lanl.gov

M. Francois
Mem. ASME
Computational Physics Division,
Los Alamos National Laboratory,
P.O. Box 1663, MS B218,
Los Alamos, NM 87544
e-mail: mmfran@lanl.gov

R. Gore
Theoretical Design Division,
Los Alamos National Laboratory,
P.O. Box 1663, MS T085,
Los Alamos, NM 87544
e-mail: rag@lanl.gov

R. Rauenzahn
Theoretical Division,
Los Alamos National Laboratory,
P.O. Box 1663, MS B216,
Los Alamos, NM 87544
e-mail: rick@lanl.gov

J. Reisner
Computational Physics Division,
Los Alamos National Laboratory,
P.O. Box 1663, MS F644,
Los Alamos, NM 87544
e-mail: reisner@lanl.gov

S. Shkoller
Department of Mathematics,
University of California, Davis,
Davis, CA 95616
e-mail: shkoller@math.ucdavis.edu

A Comparison of Interface Growth Models Applied to Rayleigh–Taylor and Richtmyer–Meshkov Instabilities

Sophisticated numerical models that contain fluid interfaces rely upon interface evolution models to approximate the transition to turbulence near interfaces, in the presence of Rayleigh–Taylor (RTI) or Richtmyer–Meshkov (RMI) instability. Semi-analytical models have been developed in recent decades to predict the interface growth from an initial state into the nonlinear regime. Two of these models are considered in this study. They are the Goncharov and the z-models. Both of these interface models have strengths and weaknesses, which are examined here. Both of them have been implemented in the xRAGE compressible flow solver, which models fluid interfaces. The flow solver provides the fluids acceleration as a body force to the interface model. The purpose of such interface model is to evolve the early times of interface position as a subgrid model within a compressible flow simulation in order to then initialize a turbulence model. In this work, the interface models are assessed and compared for their evolution of RTI and RMI. The z-model performed better than the Goncharov model for all cases that were explored.
[DOI: 10.1115/1.4048341]

Introduction

The work presented here was initiated by Dr. Malcolm Andrews at Los Alamos National Laboratory in his research on turbulence. His innovation was to calculate the initial conditions for turbulence models from semi-analytical solutions of the Rayleigh–Taylor (RTI) and Richtmyer–Meshkov (RMI) instabilities. This approach permits quantifiable, physical initial conditions that would otherwise have been crudely estimated. He titled his work "Turbulence by design."

Instabilities that develop at an interface between two fluids of different densities when the interface is accelerated can often lead to turbulent mixing. The process that evolves as the initially separated fluids become entwined is referred to as either RTI or RMI. These instabilities were named after the scientists that first published solutions to these problems [1–4]. The distinction between RTI and RMI is conditional on the nature of the accelerating force, which must be present to set the process in motion. For the case of RTI, it is a body force such as gravity. In RMI, the force is an impulsive acceleration, driven by a shock as it traverses the interface. In both cases, the force causes a pressure gradient across the interface. The pressure gradient must be misaligned with the density gradient at the interface to initiate the instability. This is

[1]Corresponding author.

Contributed by the Fluids Engineering Division of ASME for publication in the Journal of Fluids Engineering. Manuscript received September 23, 2019; final manuscript received June 23, 2020; published online October 29, 2020. Assoc. Editor: Arindam Banerjee.

visualized in Fig. 1(*a*), for RTI and Fig. 1(*b*) for RMI. The zoomed-in images of the interface in Figs. 1(*a*) and 1(*b*) show density, ρ_1, in red and density, ρ_2, as blue. The perturbations cause density gradients in the interface-parallel direction as well as the interface-normal direction. The perturbations in Fig. 1 are sinusoidal. However, the perturbations can appear in any form. The interface-normal pressure gradient for RTI, Fig. 1(*a*), is due to the hydrostatic pressure, which is piecewise continuous to either side of the interface. For the RMI case, Fig. 1(*b*), a pressure jump normal to the interface occurs when the shock briefly impinges it. For both cases, the interface-parallel density gradients and the interface-normal pressure gradients impart baroclinic vorticity on the interface. The vorticity manifests as: $\nabla\rho \times \nabla p \neq 0$ in the vorticity equation. An additional constraint for RTI is that the pressure gradient opposes the density gradient, $\nabla\rho \cdot \nabla p < 0$, because otherwise, the body force stabilizes the system and the interface will oscillate as a standing wave.

The RTI and RMI problems have been extensively researched for more than a century. The seminal works of Refs. [1–5] studied the linear regimes and are not discussed here. This work focuses on the nonlinear regime and semi-analytical models that have been developed to predict the interface growth from an initial state into the nonlinear regime [6–13].

The work of Goncharov [6] extends the model of Layzer [7] to all physical Atwood numbers. The models of Layzer and Goncharov [6,7] start with the potential flow solution of Taylor [2] and extend the evolution of η into the nonlinear regime with asymptotic perturbation methods. They expanded η about the bubble tip with power series to derive semi-analytical equations that predict the bubble height for a single-mode perturbation. Goncharov recognized that this method was valid for bubbles but not for spikes [6]. Mikaelian analyzed the Layzer and Goncharov models [8] and found that they had several modes of failure. He demonstrated the inability of the Goncharov model to predict spike growth [6,8]. Mikaelian also discovered that the model failed for initial conditions parameterized by the product of the wave number and the interface amplitude, ηk_0. If ηk_0 is greater than a value that is dependent on Atwood number, then the model fails [8]. In addition, he showed that the bubble amplitude cannot change sign. Mikaelian proposed another nonlinear, single-mode model [8] that overcomes the failures of the Layzer and Goncharov models. Zhang and Guo also improved upon the Layzer model by including an additional term, which models the higher order terms in the series expansion [9].

Haan derived a nonlinear multimode interface evolution model from the potential flow equations [10]. He accomplished this by retaining the nonlinear advection terms and expanding the interface-normal derivatives to second-order with Taylor series. The resulting equations are semi-analytical and were solved by substituting the linear solution into the nonlinear terms [10]. He showed that he could evolve interface amplitude while simultaneously evolving the energy spectra with this method. The model of Rollin and Andrews [11] combined the Goncharov and Haan models by substituting the Goncharov solution into the nonlinear Haan terms. They used a constitutive model to evolve the spikes with the Goncharov model. The constitutive model was developed by executing direct numerical simulations of RTI and tabulating multiplicative factors that relate spike height to bubble height for a range of Atwood numbers.

Granero-Belinchón and Shkoller developed two multimode interface evolution models [13]. The first model presented in Ref. [13] is similar to the Haan model in that it evolves sinusoidal interfaces into the nonlinear regime. The second model of [13] is an interface model that is nonparametric. It evolves the interface amplitude as well as the interface vorticity, which allows for the interface to roll up and exhibit the classical "mushroom" shape associated with bubbles and spikes in RTI.

These instabilities have been studied comprehensively [1–16]. Yet, modeling the early nonlinear phases of RTI or RMI, before transition to turbulence, remains a challenge. Efforts have been made to model this with direct numerical simulation and high-resolution large eddy simulations [15,16]. However, direct numerical simulations are computationally expensive and impractical to solve engineering scale problems even on today's largest super computers. Therefore, one needs to represent the evolution of fluid interfaces as a subgrid model to approximate the transition to turbulence near interfaces. The motivation for this study is to evaluate two interface evolution models for capturing the early transition to turbulence phase in RTI and RMI and compare these models to experiments.

While there are many models in the literature [6–13], in this study we only consider two of them. They are the Goncharov model [6] and the z-model of Granero-Belinchón and Shkoller [13]. In order to reference these papers throughout this document, the paper by Goncharov [6] will be referred to as G02 and the paper by Granero-Belinchón and Shkoller [13] shall be called Z17. Each of these interface models have strengths and weaknesses, which are examined here. Further these interface models are assessed and compared in the context of their coupling to a compressible fluid flow solver, xRAGE, for both RTI and RMI. To our knowledge, such coupling has not been reported

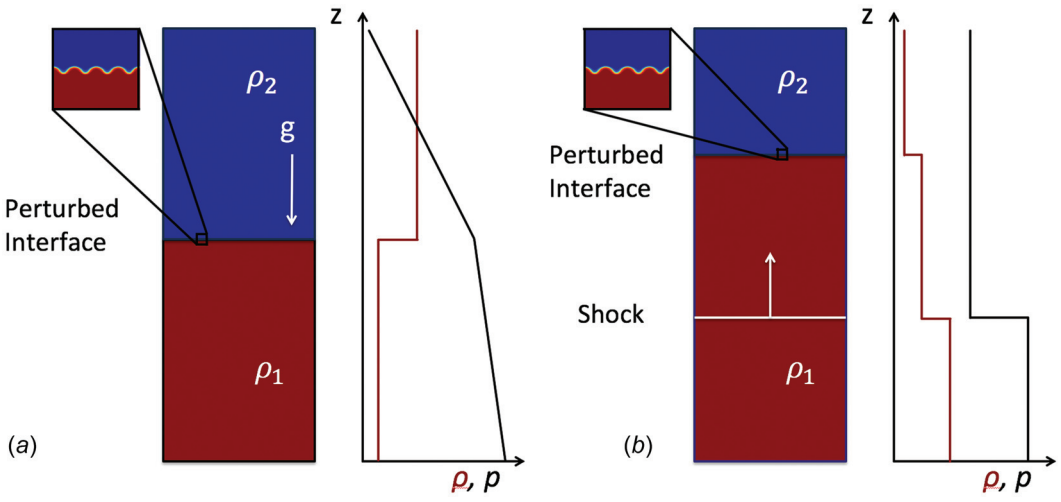

Fig. 1 (*a*) RTI and (*b*) RMI. The difference between RTI and RMI is the functional form of the acceleration driving the instability. For RTI, the acceleration is continuous in time, whereas for RMI, the acceleration is an impulse driven by a shockwave transiting the interface. The RMI acceleration is often represented mathematically as a Dirac delta function.

previously, hence, the novelty of this work. The flow solver couples to the interface models through the local acceleration at the interface. The interface model then evolves in amplitude, shape, and position and can calculate turbulence quantities for initializing a turbulence model.

The G02 model is a single-mode growth model that calculates bubble growth, but not spikes growth. It is reported to be second-order accurate [6]. The z-model of Z17 is a mode coupling, spectral model. The Z17 model predicts both bubble and spike growth. The Z17 model is not constrained to be a graph (parametric function), unlike other similar models [10]. In fact, it can develop the interface into a multivalued curve for a specific set of independent variable coordinates as the interface rolls up due to the presence of vorticity. That is to say, not only can the interface stretch and translate, it can fold over on itself, or roll up (rotate), as the dynamics dictates. This model is purported to be second-order accurate [13].

The models of G02 and Z17 are compared against RTI experiments performed by Waddell et al. [17]. The paper of Waddell et al. [17] is referred to as W01 throughout this work. The models of G02 and Z17 are also compared to RMI experiments, undertaken by Vandenboomgaerde et al. [18]. The paper by Vandenboomgaerde et al. [18] is referred to as V14. These experiments were chosen for this study for multiple reasons. They represented two instabilities, RTI and RMI. Both experiments detail single-mode initial conditions that evolve into multimode states. The initial conditions were well resolved and characterized for both experiments. Finally, the resulting data from each experiment provided sufficient resolution to do the model comparisons.

The paper is organized in the following way. In the Cases Considered section, cases considered, the RTI experiments of W01 and the RMI experiments of V14, are described. The interface models section introduces the G02 model first and then presents the Z17 model. Then, the numerical methods used to solve the interface models are described. Next, the flow solver is introduced and a description of the coupling between the interface models and the flow solver is given. The Results and Discussion section provide a detailed comparison of the models of G02 and Z17 with the RTI experiments of W01 and then the RMI experiments of V14. Finally, the salient results are summarized in the conclusion and the proposed future work is outlined.

Cases Considered

In the experiments of W01, single-mode RTI was conducted through use of a weight and pully accelerator that propelled an initially stable two-fluid system, residing on a sled, downward to achieve the instability. A Plexiglas tank, containing two liquids, occupied the sled, which was guided by a rail in the apparatus. To achieve a single-mode perturbation along the interface, a linear stepper motor agitated the tank in the horizontal direction. A motion controller was programmed to generate sinusoidal motion of the stepper motor with a precise amplitude and frequency. With this method, W01 achieved a single-mode standing wave with a measurable amplitude and frequency. A more detailed description of the apparatus can be found in W01 [17].

For the study in this paper, one of the case studies from W01 was simulated with the G02 and Z17 models. The case was a miscible system with isopropyl alcohol residing above salt water in a stable configuration. This combination of fluids is characterized by an Atwood number, $A = 0.155$. The initial perturbation consisted of an initial amplitude, $\eta_0 = 0.1$ (cm) and a wavelength of $\lambda = 5.4$ (cm). The steady acceleration was reported to be $G = 0.74$, where G is a multiplicative factor on Earth's gravitational acceleration, $g = 981$ (cm s^{-2}). For a broader description of the experiment setup, refer to W01 [17].

The V14 experiments were used to benchmark the G02 and Z17 models for RMI. In V14, shock tube experiments were conducted in a two-gas system containing shocked air expanding into sulfur hexafluoride (SF_6) with well-defined initial conditions that were numerically replicable. The shock tube cross section was 20×20 (cm^2). The initial condition of V14 was a two-dimensional (2D), cosine waveform at the interface. These experiments were run for two initial amplitudes, $\eta_0 = 0.306$ (cm) and $\eta_0 = 0.918$ (cm). The postshock amplitudes that we used were $\eta_0 = 0.28$ (cm) and $\eta_0 = 0.67$ (cm). These values were derived from digitizing the data in Fig. 5 of [18]. Everything else was fixed. The cosine wavelength was $\lambda = 8$ (cm). The air-SF_6 combination provided an Atwood number, $A = 0.679$. Finally, the shock Mach number was $M = 1.45$ with standard temperature and pressure conditions. Further details can be found in V14 [18].

The third case examined in this work was to see how the models of G02 and Z17 performed in a stable configuration for a linear standing wave as is found at the interface between the oceans and the atmosphere, for example. The parameters for this case were an initial amplitude $\eta_0 = 0.1$ (cm), wavelength $\lambda = 1$ (cm), Atwood number $A = 0.1$, and acceleration $g = 1000$ (cm s^{-2}). These parameters were chosen for the ease of deriving the analytical frequency of oscillation, $\omega_0 = \sqrt{A\,g\,k} = 25.066$ (Hz), of the interface.

These three scenarios are ideal for validating the models of G02 and Z17. Acceleration is the leading order driver in the W01 and V14 experiments, as well as the standing wave. The effects of viscosity, diffusion, and surface tension may have been present. However, these effects were not reported nor discussed in W01 or V14.

Interface Models

The two interface evolution models of G02 and Z17 under study are presented below. Details of the model derivations are not duplicated here and can be found in G02 and Z17 [6,13], respectively. Both models are semi-analytical and are used to evolve the interface at early times into the nonlinear regime. Once a sufficiently high Reynolds number, $R = \frac{\eta_k \dot{\eta}_k}{\upsilon}$ where υ is the dynamic viscosity of the fluids, has been achieved in the interface model, turbulence quantities can be calculated and used to initialize a turbulence model. For this study, R was allowed to grow arbitrarily high in order to let the interface models evolve for the duration of the experiments. For use in initializing a turbulence model, a critical value for R is set and used as a free parameter to turn the interface model off and initialize the turbulence model. The benefit of utilizing an interface model in this way is that the interface model evolves the flow field energy spectrum to a more physical initialization of the turbulence model.

The Goncharov Model. The G02 model was part of Dr. Andrews work on turbulence by design [11]. The G02 model evolves each mode independently for η_k. This means that modes do not interact with one another. The governing equations of the G02 model [6] are given by

$$F_1 \frac{\ddot{\eta}_k}{D} + F_2 \frac{c^2 k^2 \dot{\eta}_k^2}{8D^2} + 2gA\eta_2 = 0 \tag{1}$$

The coefficients, denominators, and η_2 in Eq. (1) are represented by

$$\eta_2 = -\frac{ck}{4(1+c)}\left(1 + \left[(1+c)\eta_0 k - 1\right] e^{-k(1+c)(\eta_k - \eta_0)}\right) \tag{2}$$

$$F_1 = 2A\eta_2^2 + \frac{c^2 Ak\eta_2}{2(1+c)} - \frac{c^2 k^2}{8(1+c)} \tag{3}$$

$$F_2 = 2A\eta_2^2 + \frac{k\eta_2}{(1+c)}(A + \mathrm{cA} - 2c - 1) \tag{4}$$

$$D = \eta_2 - \frac{ck}{4(1+c)} \tag{5}$$

The G02 model was presented in this form by Mikaelian [8]. It generalizes the 2D and three-dimensional (3D) cases to one set of equations by introducing the parameter c. When the 2D case is solved, $c = 2$. For the 3D case, $c = 1$. There is a difference between 2D and 3D because the model is expanded about a bubble tip, represented by a cosine function in 2D and a Bessel function in 3D [6]. Figure 2 shows the 3D bubble tip represented as the Bessel function of the first kind with integer order zero compared to a cosine waveform, for reference. In Eqs. (1)–(5), η_k is the modal amplitude, k is the modal wave number, and η_2 is the solution to the linear ordinary differential equation that arises in the asymptotic expansion about the bubble tip while deriving the Goncharov model. In Eqs. (1)–(5), $\dot{\eta}_k$ represents the first time derivative of η_k and $\ddot{\eta}_k$ represents the second time derivative of η_k. For this study, the G02 model needed to be predictive and was used for bubble and spike evolution, even though the G02 model is known to fail for spikes [6,8]. In order to model spikes for comparison with the Z17 model and the experiments of W01 and V14, $\dot{\eta}_k^2$ was replaced with $\dot{\eta}_k|\dot{\eta}_k|$ in Eq. (1).

The z-Model. The z-model of Z17 is a mode coupling interface model with three governing equations. The most prominent difference between the G02 model and the Z17 model is that the modes interact with one another in the Z17 model, whereas modes are independent of each other in the G02 model. Another difference between the G02 and Z17 models is that presently the derivation of the Z17 model has only been published for 2D interfaces. The G02 model has 2D and 3D forms. The governing equations for the z-model of Z17 are

$$\dot{\xi} = -\frac{1}{2}H(\omega)\frac{k\eta}{\|(1+k\xi, k\eta)\|} - k^2\epsilon\xi \tag{6}$$

$$\dot{\eta} = \frac{1}{2}H(\omega)\frac{1+k\xi}{\|(1+k\xi, k\eta)\|} - k^2\epsilon\eta \tag{7}$$

$$\dot{\omega} = \frac{A}{2}\frac{H(\omega H(\omega))}{\|(1+k\xi, k\eta)\|} - 2Ag\eta - k^2\epsilon\omega \tag{8}$$

In Eqs. (6)–(8), ξ is the modal amplitude of the interface-parallel position. ξ will be discussed more later. ω is the vorticity amplitude, compactly supported on the interface. Also, ω is integrated across the interface and thus has units of length divided by time. Like the G02 model, η is the modal amplitude in the interface normal direction. A dot over the dependent variable, $\dot{\eta}_k$, represents a time derivative. $H(\,)$ is the Hilbert transform operator. It is a principal value integral given by

$$H(\varphi(y)) \equiv \frac{1}{\pi}P.V.\int\frac{\varphi(y)}{y'-y}dy \tag{9}$$

$H(\,)$ is applied to a variable in Fourier space, where it is computed as a $\frac{\pi}{2}$ phase shift of that variable, rather than computing the principal value integral in real space. The denominator expression, $\|(1+k\xi, k\eta)\|$, is the slope of the interface, where the parentheses indicates a vector, i.e., $(a, b) \equiv a\boldsymbol{e}_1 + b\boldsymbol{e}_2$. The quantities A, g, and k have the same definitions as above for the G02 model. The parameter, ϵ, is a linear artificial viscosity that is included to regularize high wave number instabilities associated with the pseudo-spectral method [19]. For the case of RTI, the artificial viscosity was set to $\epsilon = 0.05$ (cm^2 s^{-1}), the same value that was used in Z17. For the RMI case, the artificial viscosity value that was used for the results presented in this paper was $\epsilon = 25.0$ (cm^2 s^{-1}). Sensitivity studies were performed, varying the value of ϵ. The sensitivity of η to ϵ was negligible for the RTI case (not shown). For the RMI case, an order of magnitude range of values of ϵ were simulated with the V14 case 1 initial conditions and the final interface amplitudes were compared to the V14 case 1 results presented in this paper. Table 1 presents the RMI sensitivity study. For the value of ϵ used for this study, the final amplitude differed by only a few percent (2.3% and 4.4%), when ϵ was reduced by half or doubled. When ϵ was increased by an order of magnitude, the final amplitude was reduced significantly (12.1% and 24.2%).

As stated above, ξ is the modal amplitude of the interface-parallel position. In real space, this is a perturbation from the fixed interface-parallel location, $\bar{x}$. We recover the real space counterpart, ξ, by performing an inverse Fourier transform on $\tilde{\xi}$

$$\xi = \frac{1}{2\pi}\int_0^\infty \tilde{\xi}e^{ikx}dk \tag{10}$$

The physical interpretation of ξ is better understood with a decomposition. Let x be the transverse coordinates of the interface. Then, we decompose x as follows:

$$x = \bar{x} + \xi \tag{11}$$

Here, $\bar{x}$ is the fixed transverse coordinates and ξ is the dynamic component of x.

The model of Z17 is a Lagrangian interface model in that the interface can translate, dilate, and rotate. These degrees-of-freedom allow for a diverse model where the interface can roll up in the presence of vorticity, a classical signature of RTI and RMI. Figure 3 shows an example of a single-mode RTI simulation with the z-model, where the initial interface is a sine wave. On the left, the early time interface contour is depicted by the blue line. As time evolves the interface grows to the red line, then the green, magenta, and finally the black line. The right figure shows evolution of the interfacial vorticity for the same times and colors as the left plot. It is apparent that as the interface evolves in time, it develops into the classical bubble (right) and spike (left) associated with RTI. It is also seen that the peak magnitudes of vorticity

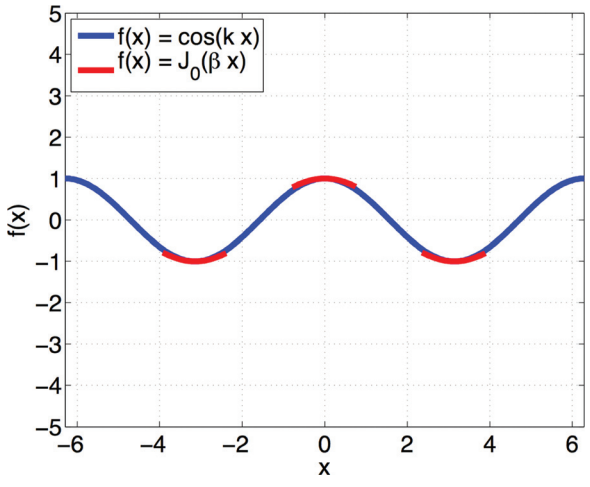

Fig. 2 The bubble tip approximation of G02 (red) for the 3D case is represented by the Bessel function near $x = 0$. The Bessel function is plotted against a cosine wave (blue) to show the similarity near the peaks and troughs of the cosine function.

Table 1 Sensitivity of final interface amplitude to artificial viscosity

ϵ (cm^2 s^{-1})	Percentage difference in final amplitude, η, from simulated cases
12.5	2.3
25.0	0.0
50.0	4.4
100.0	12.1
200.0	24.2

Note: ϵ: for the V14 RMI case.

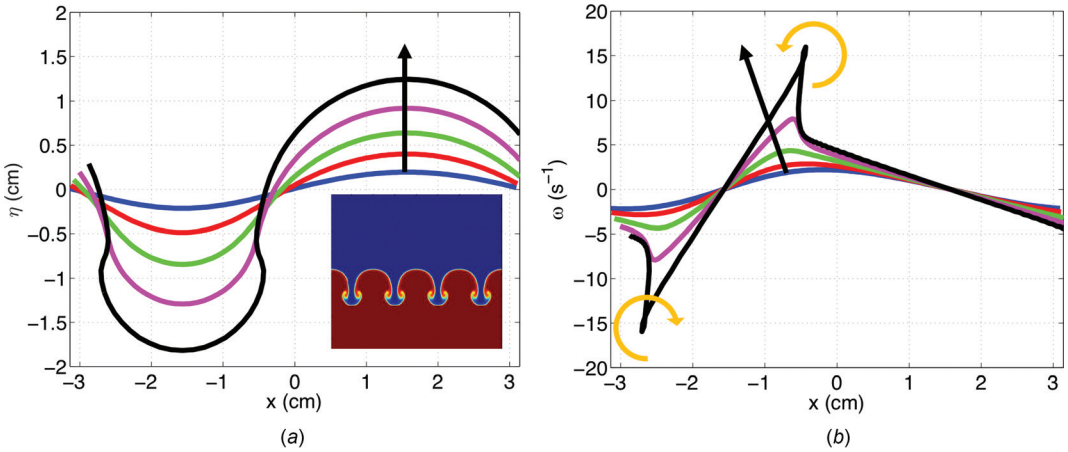

Fig. 3 Evolution of the Z17 model for an example initial single-mode sine wave with $\eta_0 = 0.1$ (cm) and $k = 1$ (cm^{-1}). Interface amplitude (*a*) is shown for 5 sequential times (blue, red, green, magenta, and black). Progression of time is indicated by the direction of the black arrow. An inset image from a single-model RTI numerical simulation is presented for qualitative comparison to the Z17 model interface. The interface vorticity (*b*) is shown for the same times (and colors). Gold circular arrows indicate the direction of rotation.

coincide with locations on the interface where roll-up has begun. Additionally, the tips of the bubble and spike coincide with zero vorticity.

Numerical Approach. Both of the models of G02 and Z17 were integrated in time with the fourth-order Runge–Kutta algorithm. The spatial component of the Z17 model was calculated with a pseudo-spectral method using fast Fourier transforms (FFT). These models were implemented in the xRAGE compressible flow solver, which is a numerical model of the Euler equations. Details of xRAGE are described in Gittings et al. [20]. The flow solver is coupled to the interface models through the flow acceleration and density fields. The local time-dependent acceleration is calculated via forward-in-time finite difference of the velocity field. The Atwood number is computed at the interface from the material densities from xRAGE, which is a multimaterial model. The acceleration and Atwood number are then transmitted to the interface model and serve as a body force to the governing equations. The interface models, which are tracked through the xRAGE mesh with Lagrangian tracers, are updated in this way for each time cycle. The models of G02 and Z17 are passive to the flow fields while the interface evolves. But, once the critical Reynolds number is reached, the turbulent length scale and turbulent kinetic energy are calculated from the interface amplitudes and velocities to initialize a turbulence model, which is directly coupled to the flow solver.

Convergence studies of the models of G02 and Z17 were performed and are briefly summarized. The G02 model, ordinary differential equations in time are sufficiently converged because the size of the time-step is determined by the compressible flow solver of xRAGE. For the model of Z17, the same time-step restriction applies as for the G02 model. For spatial convergence of the Z17 model, a number of simulations were performed starting with 16 modes and doubling the resolution up to 2048 modes for a simple RTI setup. The model was converged with 128 modes for a sufficient length of time to simulate the experiments of W01 and V14. However, 256 modes were used for the studies reported here. For the RMI cases, the presence of shocks in xRAGE does not result in convergence issues because the calculated acceleration feeds into the interface models. A time resolution study was performed on the calculated acceleration. The acceleration was integrated in time to determine the impulse from the shock. When the impulse did not change with respect to decreasing time-step, the acceleration was deemed to be converged. The acceleration was converged for the time-steps used in these studies. Convergence of the acceleration was performed with the interface models for simulations of the V14 experiments (not shown).

Results and Discussion

Rayleigh–Taylor Instability Case. In Fig. 4, PLIF images from W01 [17] are shown with the Z17 model interface superimposed on top of the images. Here, the times reported in W01 as well as the times from the simulation are placed on each image. The acceleration profile from Fig. 5 (below) was used for the Z17 model simulation in Fig. 4. The Z17 model does remarkably well at capturing the geometry and amplitude of the interface. In fact,

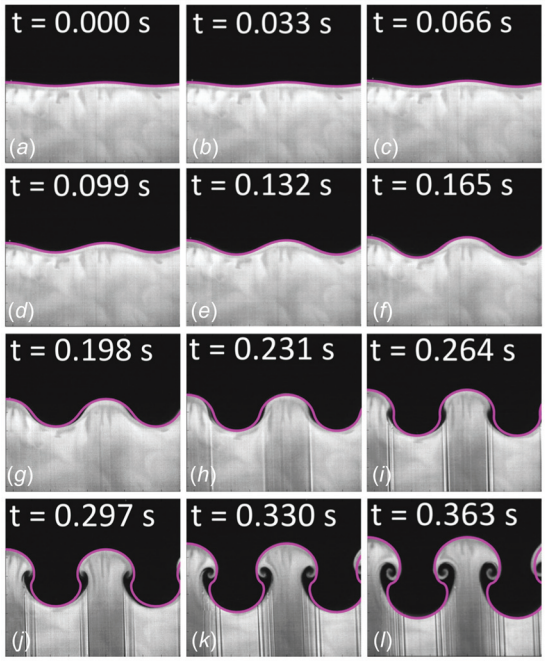

Fig. 4 The Z17 model interface amplitude (magenta) overlaying PLIF images of experiment results from Fig. 4 of W01 (Reproduced with permission from Ref. [17]. Copyright 2001 by AIP Publishing). Times for both simulation and experiment are given at the top, (*a*)–(*l*). The acceleration profile from Fig. 5 was used for the Z17 model simulation.

bubbles and spikes evolve for the Z17 model in conjunction with the experiment of W01. The final time shows an excellent comparison, exhibiting the classical mushroom shaped bubbles and spikes. However, the Z17 model does not capture the full roll-up of the interface. This is a limitation of the pseudo-spectral method, rather than a deficiency of the Z17 model. Recent work [21] has addressed improving the interface roll-up of the Z17 model.

Figure 6 shows the half-mix widths, measured from bubble tip to spike tip for the constant mean acceleration, $G = 0.74$ reported in W01. The W01 experimental results are given by the black dots, the G02 model results are represented by the red curve, the blue curve presents the Z17 model, and the linear solution is given by the green curve. With the constant acceleration, both the G02 and Z17 models underpredict the growth rate in the linear regime (early time) and overpredict the growth rate in the nonlinear regime (late time), compared to the experiment. Root-mean-square errors (RSMEs) were calculated with simulation results treated as the estimator. The RSMEs are presented in Table 2. RSMEs were 0.171 (cm) and 0.280 (cm) for the GO2 and Z17 results, respectively, in Fig. 6. The linear solution grows with comparable rates to the G02 and Z17 models for early times before diverging on an exponential growth trajectory. Even though the models of G02 and Z17 grow the interface slower than the W01 experiments early on, the faster growth rate at late times causes the interface amplitude to catch up to the experimental amplitude and for the case of the G02 model, the interface has grown larger than in the experiment for late times.

To better understand the discrepancy between the W01 experiment growth rates and those of the G02 and Z17 models, a case with a variable acceleration was simulated, which was digitized from the early time acceleration reported in W01. Figure 5 shows the measured acceleration from the W01 experiment, up to $t = 0.14$ (s), as the black solid curve. The dashed red curve is the digitized approximation of the black curve and represents the modeled acceleration used below, in the simulations of Fig. 7. The acceleration was digitized up to $t = 0.1$ (s) to capture the initial low-mode oscillations. Then, a constant acceleration of $G = 0.6$ was used. The late-time acceleration, $G = 0.6$, was used instead of the reported constant mean, $G = 0.74$, because the early time, digitized acceleration was more than twice the reported mean for the duration and influenced the late-time interface growth. W01 reported that the low-mode oscillations were the result of elastic deformations of the cables used to accelerate the test section. Upon driving the models of G02 and Z17 with the digitized acceleration, it was observed that the early time growth rates of the simulations were in much better agreement with the W01 experiments than when the constant acceleration was used.

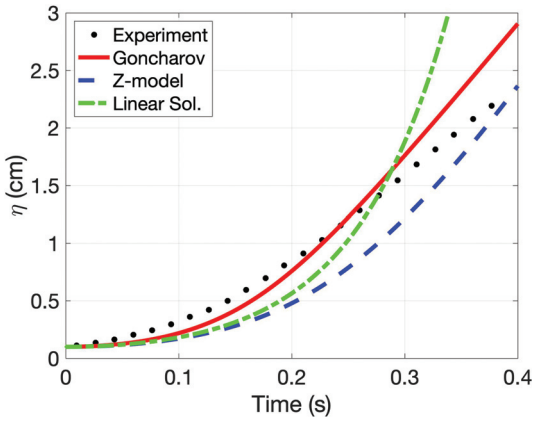

Fig. 6 Time series of the maximum G02 (red) and Z17 model (blue) amplitudes compared to the experiments of W01 (black dots), miscible case, and the linear analytical solution (green). For this case, the constant acceleration, $G = 0.74$, reported by W01 was used for the simulations and linear solution.

Table 2 RSME for the W01 and V14 comparisons in Figs. 5, 7, and 11

RSME	Goncharov	z-model
Figure 5 (W01)	0.171 (cm)	0.280 (cm)
Figure 7 (W01)	0.434 (cm)	0.096 (cm)
Figure 11, case 1 (V14)	0.325 (cm)	0.187 (cm)
Figure 11, case 2 (V14)	0.356 (cm)	0.190 (cm)

The early time higher amplitude growth rate from the W01 experiment is accounted for by the two acceleration peaks, seen in Fig. 5, due to the stretching cable. These peaks are impulses that, analogous to the extreme case of RMI, cause the interface to grow at a certain rate dependent on the impulse magnitude and duration. As the cable rebounded from being stretched, the interface continued to grow at a rate determined by the impulse peak. Simulations with both the G02 and Z17 models, not shown, were performed with the initial impulse, but not the second. These simulations matched the early growth rates of the experiment, but not the late-time growth rate. It was not until the second impulse was also included in the simulations that the early- and late-time growth rates compared well with the W01 results as shown by Fig. 7. The simulations in Fig. 7 do not exactly produce the growth rates

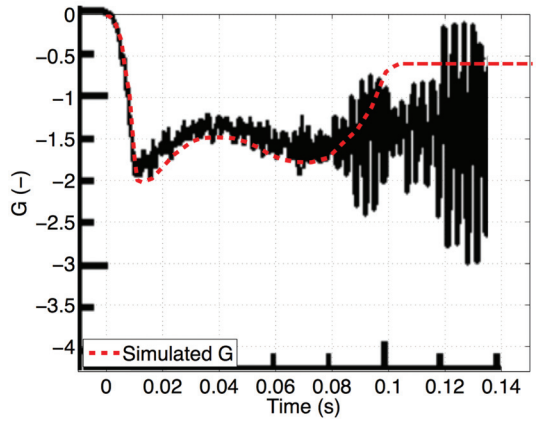

Fig. 5 Digitized early time acceleration (dashed red line), $G = f(t)$, overlaying the measured acceleration (black) in Fig. 2 of W01 (Reproduced with permission from Ref. [17]. Copyright 2001 by AIP Publishing). After $t = 0.1$ (s), the digitized acceleration was relaxed to a constant acceleration, $G = 0.6$.

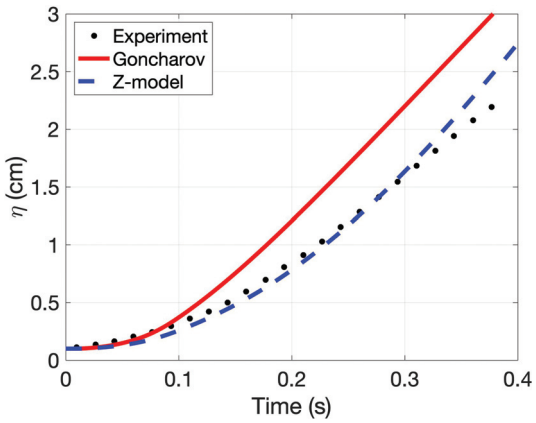

Fig. 7 Time series of the maximum G02 (red) and Z17 (blue) model amplitudes compared to the experiments of W01 (black dots), miscible case. For this case, a digitized acceleration, $G = f(t)$, from Fig. 2 of W01 was used for the simulations. The digitized acceleration is presented in Fig. 6 of this paper.

observed in the experiments of W01; however, the modeled amplitudes are in better agreement with the experiments than the simulations displayed in Fig. 6. Finally, with the variable acceleration of Fig. 7, the Z17 model reproduces the amplitude of the W01 experiment better than the model of G02. This is because the G02 model has no mechanism to allow the interface to roll up, nor does it model mode-coupling to cascade energy to smaller scales. Thus, while the G02 model reproduced the growth rates of the W01 experiment, it overpredicted the amplitude at late times, whereas the model of Z17 evolves vorticity and models mode-coupling, which are both present in the W01 results. RSMEs were 0.434 (cm) and 0.096 (cm) for the GO2 and Z17 results, respectively, in Fig. 7.

Figure 8 is the same PLIF image from the last panel of Fig. 4. However, the G02 model results have been overlaid on top of the image as well as the Z17 model results. Figure 8 illustrates that, since the G02 model can only evolve the tip of the bubbles [6,8], it has no information about the interface between the bubble and spike tips. In addition, the G02 model has no mechanism for the curvature of the bubble to change sign [8] and it is always represented by a Bessel function (for 3D). This will be discussed in more detail in regard to the standing wave problem.

Richtmyer–Meshkov Instability Case. Two cases were run from the V14 experiments. Case 1, Fig. 9, shows laser sheet images from the low amplitude case, where, $\eta_0 = 0.28$ (cm). Z17 results are superimposed on top of the laser sheet images. Once again, the Z17 model evolves to capture both the mixing layer growth as well as the interface geometry. Case 2, Fig. 8, depicts the large amplitude case, $\eta_0 = 0.67$ (cm). The first panel of Fig. 10 contains a laser sheet image of the preshock initial condition. This is mismatched with the Z17 model interface overlaid on the image because the Z17 model was initialized with the post-shock amplitude. Much like case 1 and the W01 experiment comparison, the Z17 model continues to perform well and predicts the mixing layer growth rate as well as the interface geometry. Figure 11 shows the half mix width for case 1 and case 2 of V14 compared against the G02 and Z17 models. The V14 experiment results are given by the black dots. The solid red line represents the G02 model and the blue dashed lines depict the half-mix width for the Z17 model. In general, the G02 model overpredicts the mix-width compared to the V14 results. The probable reason for the overprediction is that the G02 model has no mechanism for the interface to turn over on itself and roll up. It can only grow the bubble tip and kinetic energy cannot dissipate to heat through vortical roll-up. However, the Z17 model can roll up the interface and demonstrates better agreement with the data of V14. For case 1, RSMEs were 0.325 (cm) and 0.187 (cm) for the GO2 and Z17 results, respectively. For case 2, RSMEs were 0.356 (cm) and 0.190 (cm) for the GO2 and Z17 results, respectively, in Fig. 11.

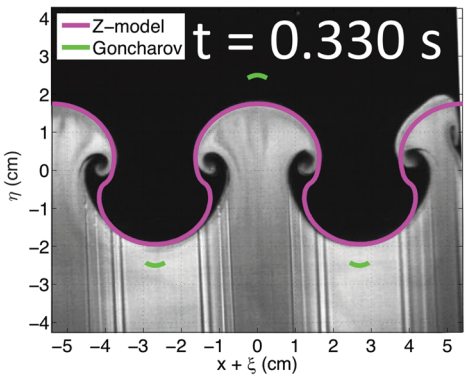

Fig. 8 Late-time comparison of the modeled interfaces of the G02 (green) and Z17 (magenta) models superimposed upon a PLIF image from Fig. 4 of W01 (Reproduced with permission from Ref. [17]. Copyright 2001 by AIP Publishing) at the same time.

There is likely an amount of uncertainty with the experimental data too. Error bars were included on the plots in V14 [18], but quantities were not reported associated with the error bars. To this end, Fig. 12 shows the Z17 model bubbles (solid blue lines) and spikes (red dashed lines) with the data of V14 laying within the bounds of the bubble and spike amplitudes of the Z17 model. Since only the half-mix widths were reported and the bubbles and spikes grow at different rates and the experimental data are bounded by the Z17 model results, excluding early time, we believe that the Z17 model produces good agreement with the experiments. As noted above, viscous and diffusion effects were not reported for the experiments of W01 or V14. These effects may contribute to differences between modeled and experimental results.

Next, the standing wave results are presented. Figure 13 shows the amplitude of a single-mode standing wave, as predicted by the models of G02 and Z17, for some time. The standing wave is in the linear regime and has an analytical solution that is readily derived. It is described earlier in the Cases Considered section. The most prominent difference between the G02 and Z17 models in Fig. 13 is that the amplitude for the G02 model grows in time while the amplitude of the Z17 model is bounded by the initial amplitude. The reason for this is that the G02 model has no physical mechanism for the bubble curvature to change signs [8]. In fact, if we let $\eta_k = 0$ from Eq. (2), indicating that the bubble is inverting or changing phase, then

$$\eta_2(\eta_k = 0) = -\frac{ck}{4(1+c)}\left(1 + \left[(1+c)\eta_0 k - 1\right]e^{k(1+c)\eta_0}\right) \quad (12)$$

and $\eta_2 < 0$, for all time, i.e., the bubble curvature, $R = -\frac{1}{2\eta_2}$, does not change sign. This result was first reported by Mikaelian [8]. We attempted to bypass this limitation by artificially changing the sign of $\dot{\eta}_k$ and η_2, when η_k changes sign and let the model continue to evolve. However, this does not let the model evolve freely. Nonetheless, we ran the G02 model with the modifications on the standing wave problem. However, during the standing wave bubble inversion, $\dot{\eta}_k$, has a maximum value. Thus, the G02 model effectively has an initial bubble velocity, $\dot{\eta}_k$. Additionally, η_0 has a fixed value which appears in the analytical solution, η_2. The combination of η_0 and $\dot{\eta}_k$ in the model, results in an overprediction of the maximum bubble amplitude, η_k, for that phase of the standing wave. The second issue that stands out in Fig. 13 is that the frequency of the G02 model decreases in time as the amplitude grows. This is a side effect of the unphysical growth of η_k in time. The analytical and model frequencies are summarized in Table 3.

Figure 14 gives an example of a multimode simulation with the z-model of Z17. The same parameters as those from the W01 experiment were used for A, g, and η_0. However, a flat spectrum of 6 modes was initialized for wave numbers ranging $1.298 < k < 4.544$ (cm^{-1}). In Fig. 12, the interface at early time is given by the black line. The blue, red, and magenta lines are chronologically later in time. This plot demonstrates that the Z17 model has multimode capability.

Conclusion and Future Work

In this study, two interface evolution models were compared against RTI and RMI experiments as well as a standing wave problem for which an analytical solution has been derived. Both the Goncharov [6] (G02) and the Granero-Belinchón and Shkoller [13] (Z17) models perform well for predicting the growth of the mixing layer in RTI and RMI. The Z17 model is able to capture both mixing layer growth rates and interface amplitudes for RTI and RMI. The G02 model replicates mixing layer growth rates. It was found that the model of Z17 could reproduce the standing wave. However, the G02 model failed to predict the standing

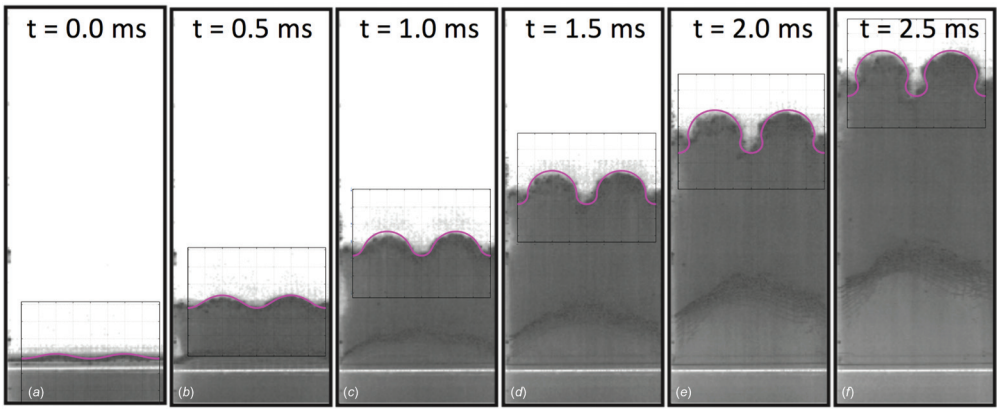

Fig. 9 The Z17 model interface amplitude (magenta) overlaying laser-sheet photography images of experiment results from Fig. 3 of V14 (Reproduced with permission from Ref. [18]. Copyright 2014 by AIP Publishing) for case 1 $\eta_0 = 0.28$ (cm). Times for both simulation and experiment are given at the top, (*a*)–(*f*).

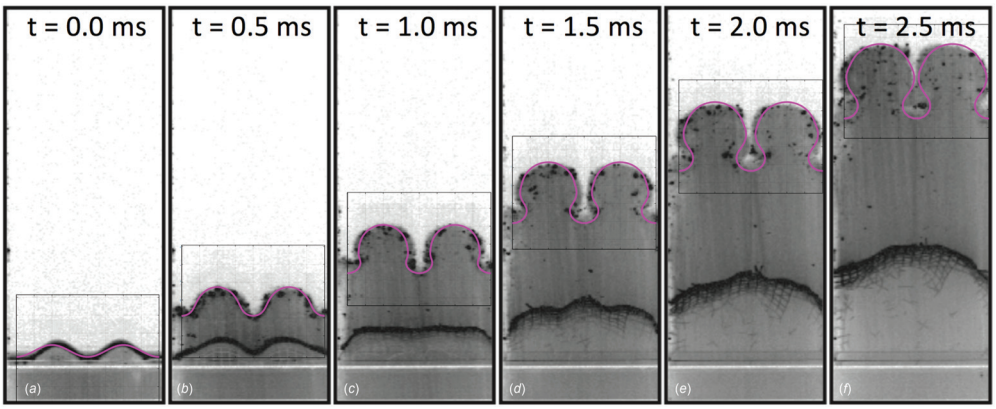

Fig. 10 The Z17 model interface amplitude (magenta) overlaying laser-sheet photography images of experiment results from Fig. 3 of V14 (Reproduced with permission from Ref. [18]. Copyright 2014 by AIP Publishing) for case 2, $\eta_0 = 0.67$ (cm). Times for both simulation and experiment are given at the top, (*a*)–(*f*).

wave amplitude and oscillation frequency. Further modification of the G02 model might fix this deficiency. The model of Z17 outperforms the model of G02 in every case examined here. Table 4 outlines the capabilities of the G02 and Z17 models.

In future work, we plan to improve both models. In particular, we plan to investigate the Goncharov approach with inclusion of interface roll-up effects, as it would be advantageous given the computational efficiency of the model. We will also investigate the model of Mikaelian [8]. The Mikaelian model does not suffer from the same limitations as the Goncharov model. For instance, it can model the standing wave problem without issue.

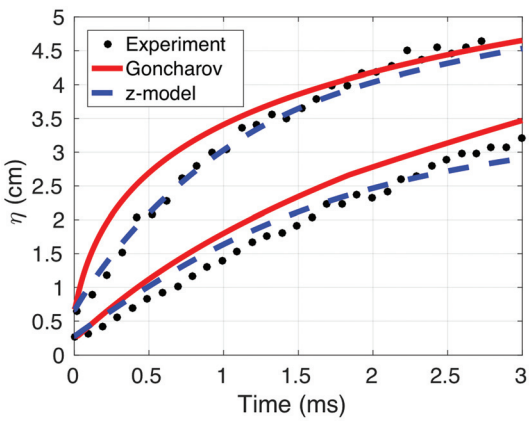

Fig. 11 Time series of the maximum G02 (red) and Z17 (blue) model amplitudes compared to the experiments of V14 (black dots)

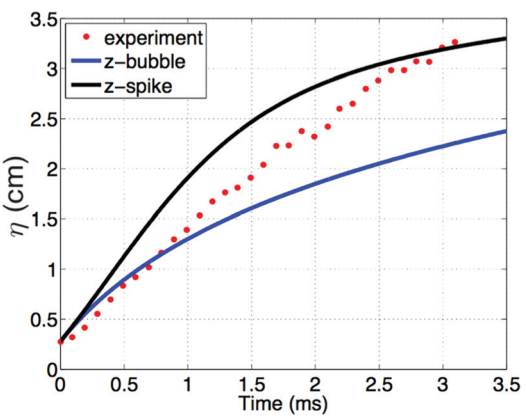

Fig. 12 The Z17 model bubble (blue) and spike (black) comparison with the case 1 experiment of V14 (red dots), showing spread of data between modeled bubbles and spikes

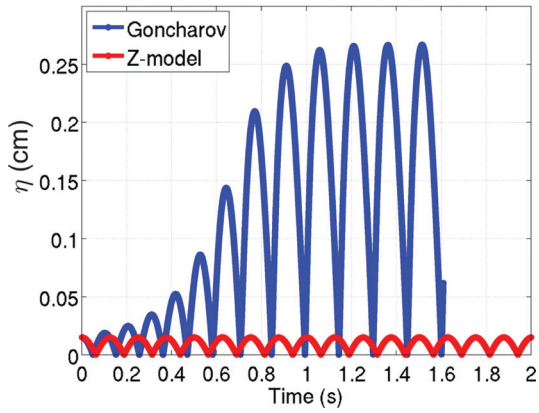

Fig. 13 The G02 (blue) and Z17 (red) models compared for the linear standing wave problem

Table 3 Standing wave comparison

Model	Frequency, ω_0 (hz)
Analytical, $\omega_0 = \sqrt{A\,g\,k}$	25.066
G02	28.274–39.270
Z17	25.133

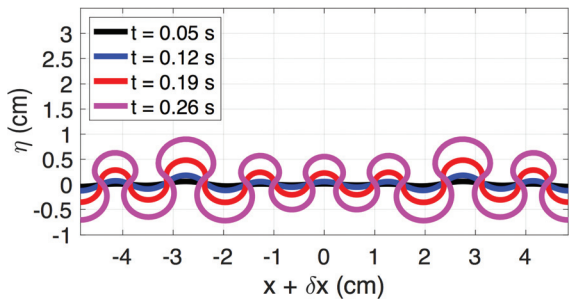

Fig. 14 Demonstration of a multimode initial condition with the Z17 model. Times are represented by black, blue, red, and magenta lines, consecutively.

New generations of the z-model have recently been derived, for example in the study of Ramani and Shkoller [21]. In Ref. [21], a "higher-order" z-model has been developed that extends the amount of interface roll-up that can be modeled and has been shown to give better agreement with W01 than Z17 does. The work of Shkoller [21] extends the z-model to a hybrid z-model/compressible Euler approach, where the velocity field of the Euler equations has been decomposed into its compressible and incompressible parts. Future efforts will involve investigating the hybrid approach of Shkoller [21]. Also, extending the z-model to higher dimensions is of interest.

Table 4 Qualities of the G02 and Z17 models

	Goncharov	z-model
Numerical stability	✓	✗
Cost (operations)	O(N)	O(N log(N))
Interface geometry	✗	✓
Three-dimensional	✓	✗
Bubbles	✓	✓
Spikes	✗	✓
Mode coupling	✗	✓
Rayleigh–Taylor	✓	✓
Richtmyer–Meshkov	✓	✓
Standing wave	✗	✓

Acknowledgment

This work was funded by the Physics and Engineering Models element of the Advanced Simulation and Computing (ASC-PEM) Program at Los Alamos National Laboratory (LANL), operated by the Department of Energy (DOE) and managed by TRIAD National Security, LLC, Contract No. 89233218CNA000001. The authors also wish to thank the High Performance Computing (HPC) division at LANL for maintaining a world class, state-of-the-art computing facility and providing exceptional support.

Funding Data

- Department of Energy (DOE) managed by TRIAD National Security, LLC, Contract No. 89233218CNA000001 (Funder ID: 10.13039/100000015).

Nomenclature

a = generic variable
A = Atwood number
b = generic variable
c = dimensionality parameter in Goncharov model
D = denominator in Goncharov model
$\boldsymbol{e}_j$ = unit vector in direction j
F_j = coefficients from Goncharov model, $j = 1, 2$
g = acceleration
G = scaling factor on Earth's gravitational acceleration for W01 experiment
G02 = Goncharov model
$H(\,)$ = Hilbert transform for z-model
i = imaginary number, $\sqrt{-1}$
k = wave number
M = Mach number
p = pressure
PEM = physics and engineering models
$P.V.\int(\,)dy$ = principal value integral for z-model
SF_6 = sulfur hexafluoride
t = time
V14 = Vandenboomgaerde et al. [18] experiments
W01 = Waddell et al. [17] immiscible experiment
x = interface-parallel coordinate for z-model
$\bar{x}$ = mean or fixed interface-parallel coordinate for z-model
Z17 = z-model
ϵ = linear artificial viscosity for z-model
η = interface amplitude for z-model
η_k = modal amplitude for Goncharov model
η_0 = initial interface amplitude
η_2 = linear solution of asymptotic expansion for Goncharov model
λ = interface wavelength
υ = dynamic viscosity
ξ = modal amplitude of interface-parallel position for z-model
$\tilde{\xi}$ = Fourier transform of ξ
ρ = fluid density
ρ_j = density of fluid $j = 1, 2$
φ = generic variable
ω = vorticity amplitude for z-model

References

[1] Strutt, J. W., 1883, "Investigation of the Character of the Equilibrium of an Incompressible Heavy Fluid of Variable Density," Proc. London Math. Soc., **14**(1), p. 8.
[2] Taylor, G. I., 1950, "The Instability of Liquid Surfaces When Accelerated in a Direction Perpendicular to Their Planes—I," Proc. R. Soc. A, **201**(1065), pp. 192–196.

[3] Richtmyer, R. D., 1960, "Taylor Instability in Shock Acceleration of Compressible Fluids," Commun. Pure Appl. Math., **13**(2), pp. 297–319.
[4] Meshkov, E. E., 1972, "Instability of the Interface of Two Gases Accelerated by a Shock Wave," Fluid Dyn., **4**(5), pp. 101–104.
[5] Chandrasekhar, S., 1981, *Hydrodynamic and Hydromagnetic Stability*, Dover, New York.
[6] Goncharov, V. N., 2002, "Analytical Model of Nonlinear, Single-Mode, Classical Rayleigh-Taylor Instability at Arbitrary Atwood Numbers," Phys. Rev. Lett., **88**(13), p. 134502.
[7] Layzer, D., 1955, "On the Instability of Superposed Fluids in a Gravitational Field," Astrophys. J., **122**(1), pp. 1–12.
[8] Mikaelian, K. O., 2008, "Limitations and Failures of the Layzer Model for Hydrodynamic Instabilities," Phys. Rev. E, **78**(1), p. 015303.
[9] Zhang, Q., and Guo, W., 2016, "Universality of Finger Growth in Two-Dimensional Rayleigh–Taylor and Richtmyer–Meshkov Instabilities With All Density Ratios," J. Fluid Mech., **786**, pp. 47–61.
[10] Haan, S. W., 1991, "Weakly Nonlinear Hydrodynamic Instabilities in Inertial Fusion," Phys. Fluids B, **3**(8), pp. 2349–2355.
[11] Rollin, B., and Andrews, M. J., 2013, "On Generating Initial Conditions for Turbulence Models: The Case of Rayleigh–Taylor Instability Turbulent Mixing," J. Turbul., **14**(3), pp. 77–106.
[12] Zhou, Y., 2017, "Rayleigh–Taylor and Richtmyer–Meshkov Instability Induced Flow, Turbulence, and Mixing. I," Phys. Rep., **720–722**, pp. 1–136.
[13] Granero-Belinchón, R., and Shkoller, S., 2017, "A Model for Rayleigh–Taylor Mixing and Interface Turnover," Multiscale Model. Simul., **15**(1), pp. 274–308.
[14] Mügler, C., and Gauthier, S., 2000, "Two-Dimensional Navier–Stokes Simulations of Gaseous Mixtures Induced by Richtmyer–Meshkov Instability," Phys. Fluids, **12**(7), pp. 1783–1798.
[15] Grinstein, F., 2017, "Initial Conditions and Modeling for Simulations of Shock Driven Turbulent Material Mixing," Comput. Fluids, **151**, pp. 58–72.
[16] Livescu, D., Wei, T., and Petersen, M., 2011, "Direct Numerical Simulations of Rayleigh-Taylor Instability," J. Phys., **318**(8), p. 082007.
[17] Waddell, J., Niederhaus, C., and Jacobs, W., 2001, "Experimental Study of Rayleigh-Taylor Instability: Low Atwood Number Liquid Systems With Single Mode Initial Perturbations," Phys. Fluids, **13**(5), pp. 1263–1273.
[18] Vandenboomgaerde, M., Souffland, D., Mariani, C., Biamino, L., Jourdan, G., and Houas, L., 2014, "An Experimental and Numerical Investigation of the Dependency on the Initial Conditions of the Richtmyer-Meshkov Instability," Phys. Fluids, **26**(2), p. 024109.
[19] Tadmor, E., 1989, "Convergence of Spectral Methods for Nonlinear Conservation Laws," SIAM J. Numer. Anal., **26**(1), pp. 30–44.
[20] Gittings, M., Weaver, R., Clover, M., Betlach, T., Byrne, N., Coker, R., Dendy, E., Hueckstaedt, R., New, K., Oakes, W. R., and Ranta, D., 2008, "The RAGE Radiation-Hydrodynamic Code," Comput. Sci. Discovery, **1**(1), p. 015005.
[21] Ramani, R., and Shkoller, S., 2020, "A Multiscale Model for Rayleigh-Taylor and Richtmyer-Meshkov Instabilities," J. Comput. Phys., **405**, p. 109177.